Theor Chem Acc (2010) 127:271–284
DOI 10.1007/s00214-010-0770-2

FEATURE ARTICLE

Theoretical advances in the dissolution studies of mineral–water interfaces

Shikha Nangia · Barbara J. Garrison

Received: 13 March 2010 / Accepted: 18 May 2010 / Published online: 6 June 2010

Abstract This article presents theoretical advances in computational modeling of dissolution at mineral–water interfaces with specific emphasis on silicates. Two different Monte Carlo methods have been developed that target equilibrium properties and kinetics in silicate–water dissolution. The equilibrium properties are explored using the combined reactive Monte Carlo and configurational bias Monte Carlo (RxMC-CBMC) method. The new RxMC-CBMC method is designed to affordably simulate the three-dimensional structure of the mineral with explicit water molecules. The kinetics of the overall dissolution process is studied using a stochastic kinetic Monte Carlo method that utilizes rate constants obtained from accurate ab initio calculations. Both these methods provide important complementary perspective of the complex dynamics involving chemical and physical interactions at the mineral–water interface. The results are compared to experimental and previous computational data available in the literature.

Keywords Dissolution · Reactive Monte Carlo · Mineral–water interfaces · Kinetic Monte Carlo · Silicates · Quartz

1 Introduction

The chemistry at the mineral–water interfaces plays a significant role in shaping the Earth's surface through intricate processes such as corrosion, dissolution, and precipitation. Besides the inherent nature of the mineral, the dissolution process is further influenced by external factors such as temperature, pH, leaching of metal ions, organic matter, and biological activity [1–6]. Among all the minerals, silica is highly significant because the Earth's crust is predominantly siliceous and constantly interacts with water. Although numerous experimental investigations [1, 2, 6–37] of various processes at silicate–water interfaces have been done, there is a growing interest in developing computational approaches [38–50] for these processes because silicate dissolution/precipitation reactions are kinetically slow and occur on geological timescales. Consequently, experimental investigations at meaningful timescales are intractable, thus development of computational modeling techniques that can span large timescales can potentially provide insight into interfacial dissolution chemistry.

In the past two decades, computational methods have evolved from isolated small clusters calculations to long-range systems representing the bulk mineral [44, 51–55]. Each study, however, primarily focuses on only one or two aspects of the interfacial chemistry. These studies are promising but have not yet unraveled all the aspects of silicate-water interaction. The primary challenge is to design efficient computational methods that integrate the atomistic detail that is present in, for example, electronic structure calculations with overall dynamics that bridge to the extended time scales. We have attempted to provide solutions to this challenge by building on positive aspects of some of the existing computational methods and avoiding their limitations. Before continuing with the new methodology, a brief background of the existing methods that provide the foundation for the new developments along with their limitations will be presented. We focus on a few popular computational approaches as an introduction

S. Nangia (✉) · B. J. Garrison
Department of Chemistry, The Pennsylvania State University, 104 Chemistry Building, University Park, PA 16802, USA
e-mail: snangia@syr.edu

to the present theoretical development in this field. The methods include ab initio cluster calculations, molecular dynamics simulations using a reactive potential energy function, and stochastic kinetic Monte Carlo.

The ab initio dissolution studies of silicates were pioneered by Lasaga and coworkers about two decades ago using the Hartree–Fock method and a small basis set for small silicate clusters [51–54]. Since then, several new density functional methods and larger basis set calculations have been used to calculate the barrier heights of dissolution reactions [56]. Pelmenschikov et al. [41] used ab initio calculations to study dissolution reactions in β-cristobalite and proposed that dissolution occurs preferentially from less coordinated surface sites. Another study by Cristenti et al. used a protonated silicate cluster to show that dissolution at low pH range has lower barrier height than the neutral case [57]. Useful ab initio methods are limited to small-sized systems with only a few atoms, because the computational cost becomes prohibitively expensive for larger systems. The need to simulate larger systems led to the development of reactive potential energy surfaces for use in molecular dynamics methods.

A reactive multi-body potential energy function for silicate-water system was pioneered by Fueston and Garofalini (FG) [58]. This FG potential energy function has been modified for several applications over the years [38, 58–67]. Besides describing the inter- and intrasurface interactions at the interface, the FG potential energy function describes bond-breaking and bond-making processes, essential for sampling reactive events. Recently, a new FG potential energy function has been developed to describe dissociative chemisorptions of water on silica surface in presence of hydronium ions [67]. The FG potential energy function energy has been reported in detail previously and is not repeated here [49]. The MD simulations using the FG potential have shown that hydrolysis of Si–O–Si bond in silicates occurs by using a single water molecule through a pentacoordinated Si intermediate [68].

Other MD simulations have been reported where hydrolysis reactions on α-quartz surface using other potential functions were modeled [43, 66, 69, 70]. Simulations on five crystallographic faces of α-quartz were performed by Du and de Leeuw et al. [70], and they proposed that some surfaces of α-quartz were more reactive than others. Also a non-reactive potential energy function using the CHARMM force field [71] was developed to determine the equilibrium structural characteristics of the silicates [72]. The MD simulations are useful for fast kinetics studies but get computationally expensive beyond a few hundred picoseconds. The applications of MD methodology are especially limited for dissolution processes that occur on much longer timescales.

For longer timescales, Luttge et al. and other groups developed a stochastic kinetic Monte Carlo model that uses surface topography as a means to calculate the overall dissolution kinetics [42, 73–76]. Their model takes into account the differential dissolution probabilities at irregular kinks, edges, steps sites compared to terrace sites. These simulations use a three-dimensional crystal lattice and predict the growth and formation of etch pits, reactive surface area, and the overall dissolution rate. Simulations using this method have also been developed by other research groups and include a wide variety of minerals.

1.1 Challenges of dissolution studies

All the methods outlined above are limited in their applications. Some of these challenges are listed below.

1. The accuracy of small cluster ab initio data is important, and there is need to incorporate these data in a methodology that calculates the overall dissolution for extended time periods.
2. The MD simulations are efficient for a very short timescale perspective of the silicate dissolution. These time-dependent simulations, however, provide only snapshots of the overall dissolution process and cannot be affordably continued to reach equilibrium conditions.
3. The stochastic approach using kinetic Monte Carlo model is performed far from equilibrium, abandoning the molecular level mechanistic details and accuracy. Moreover, the assumptions of the method require the simulations to be calibrated against experimental data.

In our work, we have developed computational approaches to address some of the challenges in the dissolution studies. We have developed a time-independent reactive Monte Carlo and configurational bias (RxMC-CBMC) methodology [49] approach to circumvent the limitations of MD simulations and determine the equilibrium properties of the silicate–water interface. In another development, we determined reaction rate constants using cluster calculations and used them in a new kinetic Monte Carlo scheme that instead of topology, takes into account the molecular level data. We highlight the strengths of these methods through several applications in this article. The aim in all the applications is to show how the atomistic description of the system is incorporated in the methodology to affordably determine the equilibrium properties and kinetic evolution of the system for extended time scales.

The article is organized in the following sections. Section 2 provides structural details of silicate minerals. Section 3 provides the theoretical background and applications of the RxMC-CBMC method. In Sect. 4, the kinetic studies are presented that include ab initio studies,

calculation of rate constants, and the KMC methodology. The discussion of results and conclusions are provided in Sect. 5.

2 Structure and nomenclature

Silicate minerals are primarily composed of SiO_4^{4-} tetrahedral units that polymerize into chains, sheets, rings, as well as many three-dimensional frameworks. Fracturing of the bulk silicate structure exposes uncoordinated Si and O atoms on the surface that quickly interact with the surroundings and get capped by an OH group or a H atom, respectively. The silicate-water chemistry is therefore interaction of Si–OH groups with water. Based on the polymerization state of the Si atom, a naming convention has been adopted in the literature. Each Si atom is classified using the Q^i notation, where i is equal to the number of bridged Si–O_{br}–Si bonds a particular Si atom forms with its Si neighbors, and the remaining $(4 - i)$ bonds are hydroxyl groups. A Si atom embedded in the bulk, tetrahedrally bridged to neighboring Si atoms and with no hydroxyl groups is a Q^4 Si. In contrast, a silicic acid $[Si(OH)_4]$ molecule in solution with no bridged bonds and four hydroxyls is a Q^0 Si. A surface Si site with one bond Si–O_{br}–Si bond and three –OH groups is termed as a Q^1 site. Similarly, Q^2 and Q^3 sites have two and three Si–O_{br}–Si bonds, respectively.

There is another naming convention based on physical location of the Si site on the surface, such as terrace, step, edge, and kink. Topographically flat uninterrupted surfaces are terraces but due to defects or other irregularities, the crystals have kinks, edges, or steps. The edge and the kink sites can also be considered as outcrops on the surface and have lesser number of Si–O_{br}–Si bonds than a terrace Si atom. In some studies, dissolution and even crystal growth is viewed as removal or creation of the reactive outcrops at kink and edge sites.

In the literature, both naming conventions are used to describe the system, depending on the methods used to describe the system. For atomistically detailed methods, the Q^i nomenclature is more suitable to describe interactions at each surface site. In our approaches, we use both nomenclatures but we will predominantly be site specific in development and applications of our methodologies.

3 Reactive and configurational bias Monte Carlo method

We developed a probabilistic RxMC-CBMC method for studying reactive and non-reactive events at the mineral–water interface [49]. The method is based on the theoretical concepts of reactive Monte Carlo schemes [77, 78], the CBMC method [79, 80], and the work by Jakobtorweihen et al. [81] reported recently. The combined method utilizes the reactive theoretical framework of the RxMC method and the algorithmic efficiency of the CBMC method. The suite of reactions at the mineral–water is considered, and the intermolecular interactions between the solid–solid, solid–water, and water–water components are described by a multi-body potential energy function.

Studying reactive events is feasible using the RxMC method because the theoretical construct of the method conserves the number of atoms in a system rather than the identity of the individual molecules. This aspect is a necessity for reactive events because during a reaction, molecules change their identities from reactant to products by breaking and forming bonds. The challenge here is that the reactive moves do not involve single atoms but rather clusters that have dissimilar sizes.

As in a mass-balanced chemical reaction, the reactant molecules are consumed and reappear as product molecules; the RxMC method models the reaction by random deletion of the reactant molecules and insertion of the product molecules according to the stoichiometry of the reaction. The RxMC therefore requires a reactive potential energy function such that the bonds in the reactants break and form product. The task then is to define a reaction transition probability $P(\text{new} \leftarrow \text{old})$ that defines the probability of changing a stochastically selected old (reactant) configuration to a new (product) configuration. A more rigorous derivation has been presented earlier [49], but the key equation for transition probability is given as

$$P(\text{new} \leftarrow \text{old}) = e^{-\frac{1}{k_B T}(U_{\text{new}} - U_{\text{old}})} \prod_{j=1}^{N_c} \frac{N_j!}{(N_j + v_j)!} \prod_{j=1}^{N_c} q_j^{v_j} \qquad (1)$$

where U is the total potential energy, T is temperature, k_B is the Boltzmann constant, N_c is the number of components, q_j is the partition function, N_j is the number of particles, and v_j is the stoichiometry of the jth component, respectively. As the reaction proceeds, the number of the components changes from N_j to $(N_j + v_j)$. The RxMC method provides a generic expression for calculating the transition probability of any reactive system. The acceptance or rejection of a reactive trial move is determined by generating a random number γ, (between 0 and 1) and comparing to $P(\text{new} \leftarrow \text{old})$. If $P(\text{new} \leftarrow \text{old})$ is greater than γ, the trial move is accepted, else it is rejected.

The potential energy term for silicate-water system is calculated using the FG potential introduced earlier in this article [58]. The transition probability is then calculated using Eq. 1. However, if the new and the old configurations are chosen without careful consideration, it can lead to a very low-efficiency simulation. The reason is that even for the simplest dissolution reaction of Si–O_{br}–Si hydrolysis,

the silicic acid product molecule needs to be inserted successfully into the dense aqueous phase. A silicic acid molecule is typically the size of a four water molecule cluster and has low probability of insertion in bulk water without steric overlapping. The transition probability for such an insertion attempt will be very small since $e^{-\beta(U_{\text{new}}-U_{\text{old}})} \rightarrow 0$ as $U_{\text{new}} \gg U_{\text{old}}$. The size disparity of the reactant and product molecules plagues the successful application of the RxMC algorithm because almost all reactive moves are rejected. It is, therefore, necessary to combine the reactive moves with an efficient technique that overcomes the problem.

The CBMC technique provides a practical solution to carry out simulations of systems that involve components with very dissimilar densities and molecular structure. We use a "cluster move" methodology to swap equivalent volumes of material in trial moves. A useful quantity for silicate-water system is that the volume occupied by a silicic acid molecule is equivalent to a cluster of four water molecules. In trial RxMC-CBMC dissolution moves, the hydrolyzed silicic acid molecule exchanges position with a cluster of water molecules in bulk water. The overlapping water molecules are removed and then reinserted randomly back into bulk water using the Rosenbluth weighting factor [82]. The CBMC technique increases the efficiency of the simulation immensely.

3.1 Applications of the RxMC-CBMC method

3.1.1 Reaction mechanisms

The RxMC-CBMC method attempts trial moves based on the suite of reactions in a particular proposed mechanism. The method can therefore be used as a powerful analysis tool to distinguish among alternative mechanisms. The silicate dissolution mechanism is not clearly understood, and there are two distinct proposed reaction mechanisms: (a) direct and (b) stepwise dissolution. The direct mechanism has been discussed by Dove et al. as a possible "plucking off" mechanism for the removal of Q^2 sites based on their experimental observations [21]. However, they concluded that further investigative work was needed to ascertain the overall mechanism. The stepwise mechanism, on the other hand, is possibly a more realistic mechanism of sequential dissolution of a bridged Si–O–Si bond at each step. The suites of reactions for both mechanisms were developed and are discussed below.

Of the two mechanisms, the direct dissolution approach mechanism leads to removal of material from the silicate surface by simultaneously hydrolyzing all the Si–O–Si bonds that are necessary for complete removal of a randomly chosen Si site. Concurrently, water molecules equal to the number of bonds hydrolyzed are randomly selected and removed from the system. The generic equation for direct dissolution of a Q^n Si site bonded to nQ^i neighbors is

$$\left[Q^i - \mathrm{O_{br}}\right]_n - Q^n(\mathrm{s}) + n\mathrm{H_2O} \rightarrow nQ^{i-1} + Q^0(\mathrm{aq}) \qquad (2)$$

In the reaction, n water molecules are consumed and a silicic acid Q^0 molecule is formed and on the surface all the n neighbors are reduced to Q^{i-1} (one less bridged neighbor). To illustrate the mechanism, a schematic of Q^2 direct dissolution is shown in Fig. 1. Conversely, in the back reaction, the Q^0 species precipitates on the surface forming Si–O_{br}–Si bridged bonds and water molecules created in the reaction are inserted in bulk water at randomly chosen sites. For each trial dissolution step, the initial and final geometries of the system are considered to calculate the transition probability using Eq. 1 to determine whether the move is acceptable.

Further analysis of the direct mechanism is performed by designing three hierarchical schemes; Q^1-dissolution, Q^1Q^2-direct, and $Q^1Q^2Q^3$-direct dissolution. The reason behind building a hierarchical set of simulations is to use the capabilities of RxMC-CBMC method to narrow down the exact mechanism of the silicate dissolution. In the Q^1-dissolution, only the reactions on Q^1 sites are followed, whereas in Q^1Q^2-direct the dissolution of Q^2 sites is allowed in addition to Q^1-dissolution, and finally in $Q^1Q^2Q^3$-direct reaction of all surface sites is allowed. The algorithm summarizing the direct mechanism is presented in Table 1.

In stepwise dissolution, only one Si–O_{br}–Si bond is hydrolyzed in every trial move. This mechanism is straightforward, but the algorithmic protocol for this simulation requires additional information about which bond to hydrolyze if the chosen Si site had multiple Si–O_{br}–Si bonds. To perform the hydrolysis at a chosen surface site efficiently, we developed a least bridged neighbor protocol [49]. This protocol requires identifying the Q^i types of neighboring Si sites, and then selecting the Si–O_{br}–Si bond to the least bridged neighbor for hydrolysis, allowing algorithmically efficiency as fewer sterically hindered moves with low-acceptance probability events are generated. To highlight the stepwise algorithm, a schematic of a Q^2 Si site is shown in Fig. 2.

The direct and the stepwise algorithm were applied to the α-quartz-water system. α-quartz is a silicate mineral, with space group $P3_121$ and a unit cell of $a = b = 4.914$ Å, $c = 5.405$ Å dimensions, $\alpha = \beta = 90°$ and $\gamma = 120°$. In the simulation, a 12 Å radius α-quartz crystallite was enclosed in a 30 Å × 30 Å × 30 Å box of water. The temperature of the system in all simulations reported here was 500 K.

The results of the direct approach hierarchical schemes show two contrasting behaviors in which the Q^1-dissolution leads to steady state, whereas the Q^1Q^2- and the $Q^1Q^2Q^3$-direct mechanisms lead to complete dissolution.

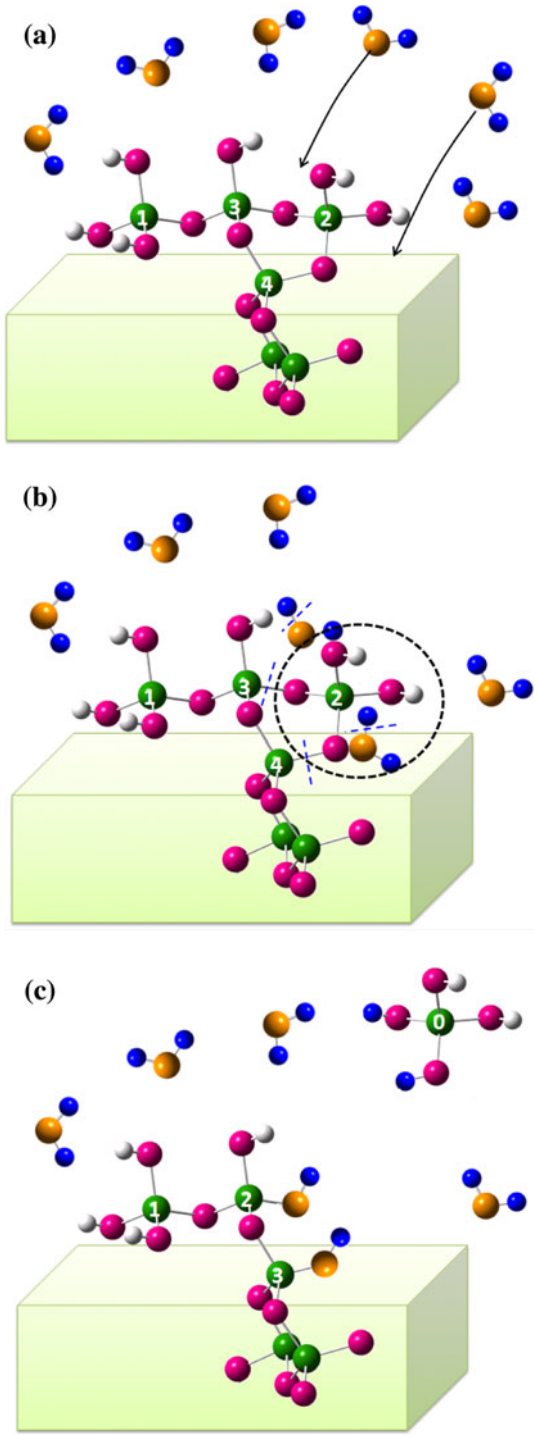

Fig. 1 Schematic of silicate crystallite surrounded by water molecules undergoing direct dissolution. The *ball* and *stick* representation of the silicate shows Si (*green*), O (*pink*) and H (*white*) and for clarity water O (*yellow*) and H (*blue*) are shown in different colors. In panel **a**, two water molecules simultaneously approach a Q^2 Si site, in **b** the bridged bonds are hydrolyzed, and in **c** the hydrolysis product Q^0 (silicic acid) moves out in solution

This result is very important from the perspective of silicate dissolution mechanism. Out of the three simulations, only the Q^1-dissolution results are in agreement with the experimental observations of reaching a steady state over extended time periods. Experimental studies have shown that quartz dissolution is kinetically a very slow process and does not lead to complete dissolution [35, 36]. In the Q^1-dissolution simulation, initially the surface Q^1 sites are removed and form the Q^0 product in solution. As the Q^0 species accumulate in solution, the probability of the precipitation reactions increases, eventually reaching a steady state. Figure 3 shows that change in the number of Q^0 species at each MC step during a Q^1-dissolution simulation. The steady state is achieved between the surface and solution after $Q^1 \leftrightarrow Q^0$ exchange reactions. Analysis of the Q^1 sites removed from the surface shows no impact of the Q^i nature of the bridged neighbor. This observation has been reported previously using ab initio calculations using silica clusters [48].

The simulation results rule out that the Q^1Q^2- and the $Q^1Q^2Q^3$-direct mechanisms as correct. This conclusion is supported by the ab initio calculations that show the gas-phase barrier height [47] for one Si–O–Si bond is 159 kJ/mol; therefore, hydrolyzing more than one bridged bonds is energetically expensive. Although the Q^1Q^2- and $Q^1Q^2Q^3$-direct dissolution approaches are potentially not the real mechanisms for dissolution of silicates, they nevertheless are useful simulations to rule out unlikely mechanisms. The question then is, does the stepwise analog of Q^1Q^2- and $Q^1Q^2Q^3$-direct mechanisms occur?

The stepwise analog Q^1 sites dissolution is the same mechanism as the direct mechanism and is called the Q^1-dissolution; however, the higher analogs are called Q^1Q^2-stepwise and $Q^1Q^2Q^3$-stepwise mechanisms. In the Q^1-dissolution, the removal of Q^1 species occurs from the surface irrespective of underlying Q^i site leading to an initial increase of Q^0 population that later plateaus to a steady-state population due to back reactions. Compared to the Q^1-dissolution simulation, the Q^1Q^2-stepwise simulation reaches a steady state in a fewer number of MC steps. The Q^2 hydrolysis is sterically difficult and results in formation of at least one Q^1 species and another Q^{i-1} species depending on the neighboring Q^i site. The same steric argument is true for Q^2 and Q^3 hydrolysis in $Q^1Q^2Q^3$-stepwise simulation and any hydrolysis that does take place leads to fluctuation of surface speciation. For comparison, the evolution of species is shown in Fig. 3 for Q^1-dissolution and $Q^1Q^2Q^3$-stepwise simulations. The most striking result of the simulations is that irrespective of the Q^1-dissolution, Q^1Q^2-, and $Q^1Q^2Q^3$-stepwise mechanisms all of

Table 1 Comparison of the dissolution and precipitation algorithms for the direct and stepwise approaches

Direct approach	Stepwise approach
Dissolution algorithm	
(a) Choose a surface Si by random selection	(a) Choose a surface Si by random selection
(b) Determine Q^i type of the selected Si	(b) Determine Q^i type of the selected Si and all its bridged Si neighbors
(c) Randomly select i water molecules in bulk water	(c) Identify the Si–O_{br}–Si bond of the chosen Si to Q^i neighbor with smallest i
(d) Delete selected i water molecules and hydrolyze i Si–O_{br}–Si bonds	(d) Randomly select 1 water molecule in bulk water, and delete
(e) Move the hydrolyzed $Si(OH)_4$ to the coordinates of one of the deleted water molecules	(e) Hydrolyze Si–O_{br}–Si bond
(f) Calculate P(step e ← step a)	(f) If Si–O_{br}–Q^1 is hydrolyzed, then move the hydrolyzed $Si(OH)_4$ to the coordinates of deleted water
(g) If P(step e ← step a) > γ, accept the move, else return to step a	(g) Calculate P(step e ← step a)
	(h) If P(step e ← step a) > γ, accept the move, else return to step a
Precipitation/polymerization algorithm	
(a) Choose a Si(aq) center by random selection	(a) Choose a Si(aq) center by random selection
(b) Randomly pick another Si center on surface or solution	(b) Randomly pick another Si center on surface or solution
(c) Move Si(aq) to the second Si to form i number of Si–O_{br}–Si bonds	(c) Move Si(aq) to the second Si to form one Si–O_{br}–Si bonds
(d) Randomly insert i water molecules in bulk water	(d) Randomly insert 1 water molecule in bulk water
(e) Calculate P(step c ← step a)	(e) Calculate P(step c ← step a)
(f) If P(e ← a) > γ, accept the move, else return to step a	(f) If P(e ← a) > γ, accept the move, else return to step a

them yield almost the same Q^0 fraction in solution and Q^4 fraction in bulk. The differences in the three mechanisms are in fractions of the Q^1, Q^2, and Q^3 surface species. These can be explained by the disparity in the hydrolysis protocols for mechanisms, but on an average, none of these mechanisms lead to complete dissolution and all reach a steady-state dissolution state. Furthermore, this confirms that even though the Q^2 and Q^3 hydrolysis events do occur, they are compensated by the backward precipitation reactions and do not contribute significantly toward the formation of Q^0 species.

3.1.2 *Interfacial studies*

We used the RxMC-CBMC method to understand another aspect of silicate-water chemistry, in which the Si surface sites on crystallographic faces of β-cristobalite (a polymorph of quartz) tend to form hydrogen bonds with their neighbors through intrasurface H-bonding, leading to tessellated patterns in some cases [44, 50, 55, 83]. In our earlier work, we established that the extent of tessellation is controlled by the types of Q^i sites predominant on the crystallographic face [50]. The results indicated that intrasurface hydrogen bonding influences the physical characteristics of the surface significantly, and therefore, an investigation of the chemical properties in these surfaces was warranted. We begin our discussion of the characteristics of the crystallographic faces of β-cristobalite by first summarizing the tessellation studies followed by the consequence of these patterns on their chemical reactivity.

The Q^i analysis of 40 unique crystallographic β-cristobalite surfaces showed that on an average, Q^3 sites are three times more abundant than the Q^2 sites, which is good agreement with experimental results [84–86]. The β-cristobalite surface can be classified into three main types, those that have (1) pure Q^3 sites, (2) pure Q^2 sites, and (3) various ratios of Q^2 sites Q^3 sites. The detailed percentage abundance of the surface sites is presented elsewhere [50].

Among all the surfaces studied, the {100} crystallographic β-cristobalite surface is unique, composed only of Q^2 sites. Both the hydroxyl groups of the surface form H-bonds with the neighbors to form an extended tessellation pattern. Despite only one pure Q^2 surface, there are nine crystallographic planes that have pure Q^3 centers. None of the pure Q^3 surfaces show intrasurface hydrogen bonding because the spacing between Q^3 sites does not allow proximity between the hydroxyl groups to form hydrogen bonds. The other surfaces with both Q^2 and Q^3 sites are qualitatively different from the others in terms of H-bonding.

Also, significant is how the β-cristobalite surfaces interact with adjacent water molecules. The results indicate

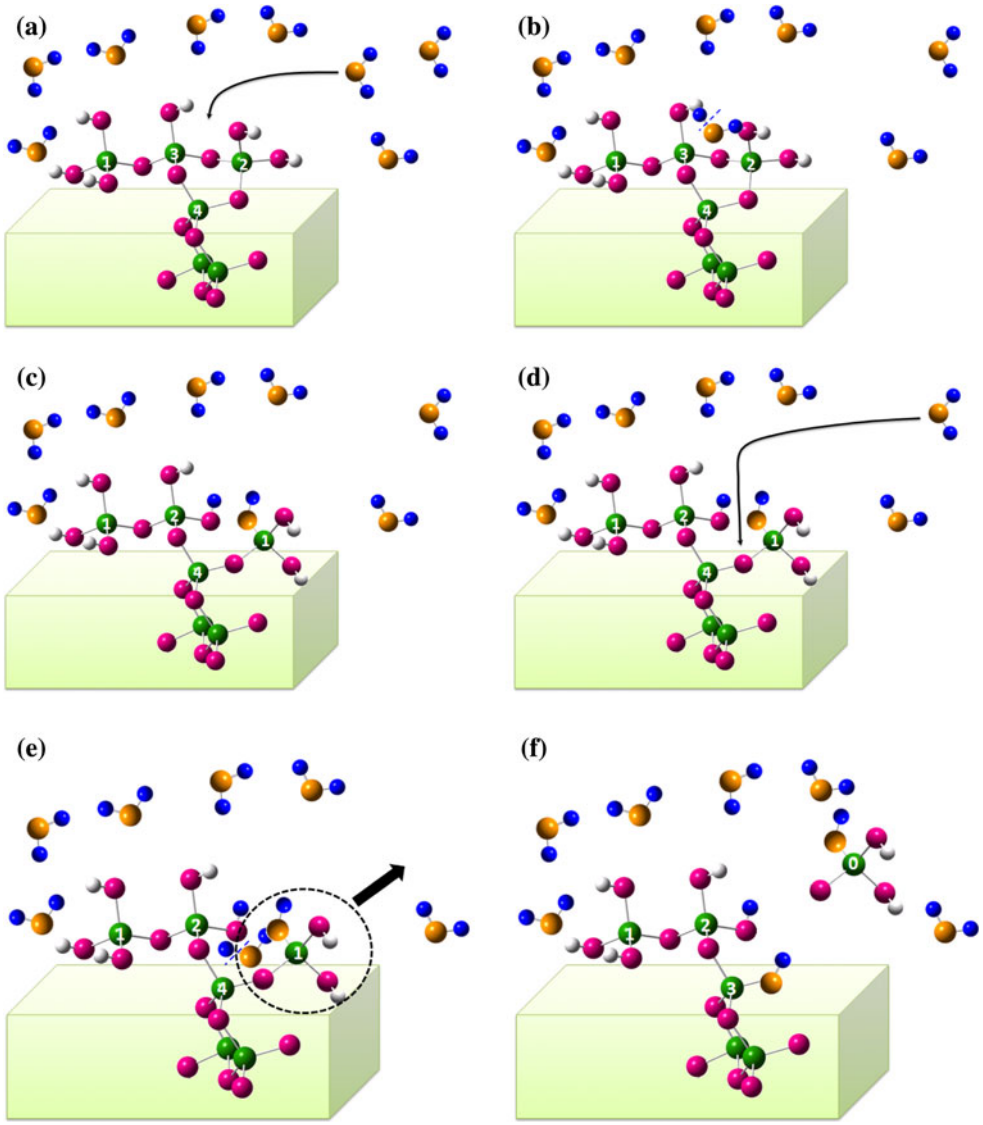

Fig. 2 A representation of silicate crystallite undergoing stepwise dissolution. The color scheme of the atoms is the same as in Fig. 1. In panel **a**, one water molecule approaches a Q^2 Si site, **b** the Q^3–O–Q^2 bridged bond is hydrolyzed, **c** the hydrolyzed Q^1 site, **d** water approaching the Q^1 site, **e** hydrolysis of the Q^4–O–Q^1 bridged bond, and **f** the stepwise hydrolyzed Si site moves out in solution as Q^0 (silicic acid)

that the {100} and {111} β-cristobalite surfaces that have ordered topology and hydroxyl groups in planes parallel to the surface adsorb water molecules through H-bonds. The {100} surface with 100% Q^2 sites has geminal hydroxyl groups in a plane parallel to the surface and forms a stable tessellated H-bond network. The {111} surface adsorbs water to form closed ring structures using two H-bonds with the surface hydroxyl groups, bridging the neighboring centers. X-ray reflectivity experiments on quartz surfaces have shown that smoothness of the surface was crucial in formation of water monolayers [87]. In Fig. 4, four crystallographic planes are shown with and without water overlayers. The figure clearly illustrates the experimental observation that only the {100} and {111} with a flat topology form extended water overlayers. The {013} and {113} surfaces with less ordered topology have only partial-ordered water overlayers.

To investigate the effect of intrasurface hydrogen bonding on chemical reactivity of the β-cristobalite surfaces, we used the $Q^1Q^2Q^3$-stepwise dissolution of the RxMC-CBMC method. Dissolution of five different surfaces with varying ratios of Q^2:Q^3 groups was simulated, and the extent of dissolution in all five cases was compared by obtaining a ratio of the number of Q^0 groups in solution divided by the number of Si sites on the initial surface until the dissolution reaches equilibrium.

A comparison of dissolution trends is plotted in Fig. 5. The results show that pure Q^3 surfaces that have no intrasurface bonding are 7–8 times more reactive than the hydrogen-bonded surface. The pure Q^3 {111} and {011} surfaces have 68–70% of their top Si layer removed by dissolution as shown in Fig. 6. The before and after dissolution images of the Si sites show that dissolution removes most of the top layer and some of the second and

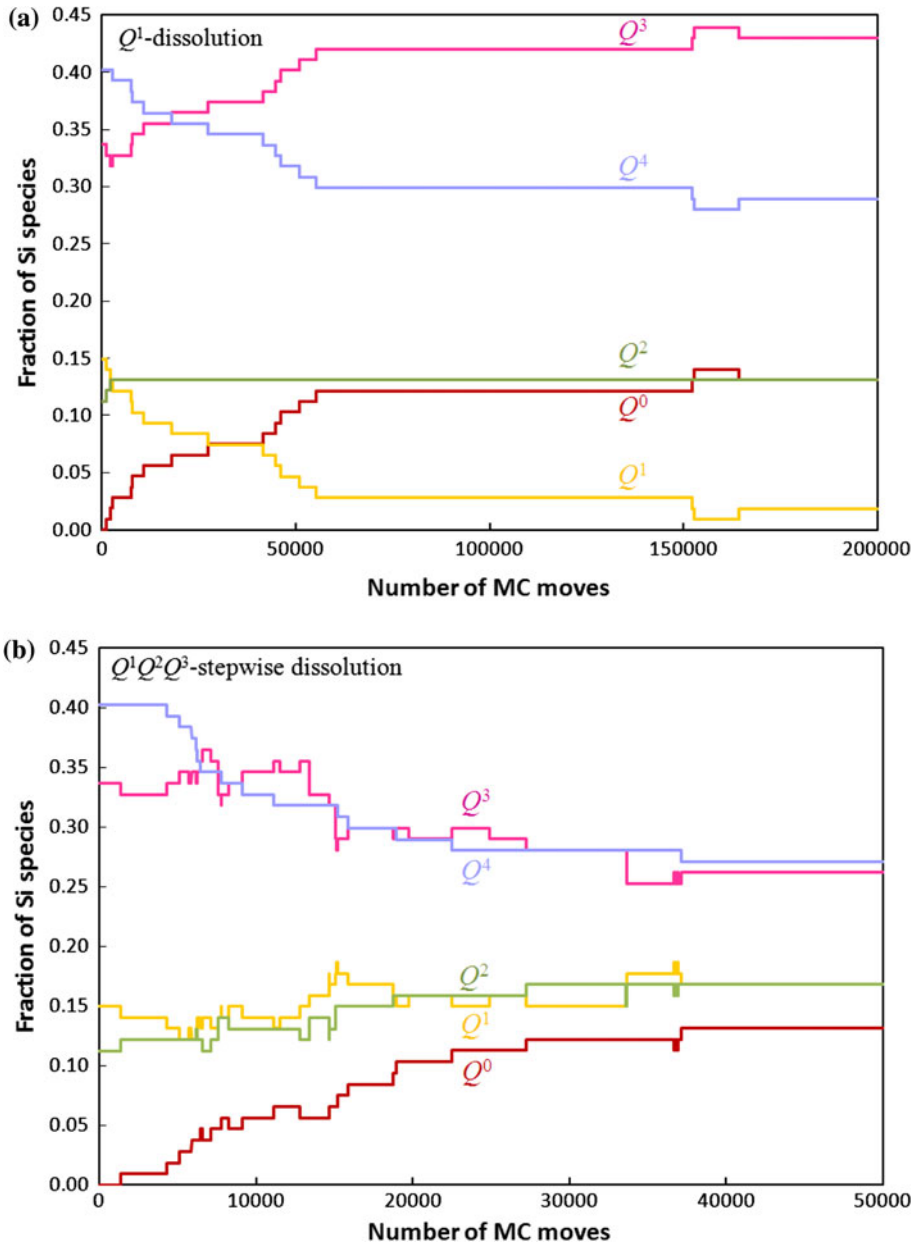

Fig. 3 Evolution of Q^i species fraction simulated using the **a** Q^1-dissolution algorithm and **b** $Q^1Q^2Q^3$-stepwise as a function of number of MC moves at 500 K

third atomic Si layers. The pure Q^2 {100} surface that is completely hydrogen bonded has limited dissolution. The surfaces with a mixture of Q^2 and Q^3 sites and less extensive hydrogen bonding have intermediate dissolution extents.

3.2 Limitations of the RxMC-CBMC

The applications of the RxMC-CBMC method have shown the strengths of the method; however, there are certain limitations of the method. Some of these limitations are inherent to the method and some are more application based, for example:

(a) The success of the method requires some initial insight into the possible reactions mechanisms and suite of elementary steps in the reaction for RxMC trail moves.
(b) The methodology provides a time-independent progression of the solid and aqueous phases during a reaction. It can estimate the concentration of the reactant and products only after equilibrium as been established.
(c) The success of the present RxMC-CBMC method relies on the potential energy function used in a particular application. In the present case, the Feuston–Garofalini potential that was employed

Plane	Composition	Surface topography	Water overlayers
100	Pure Q^2	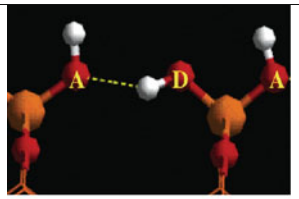	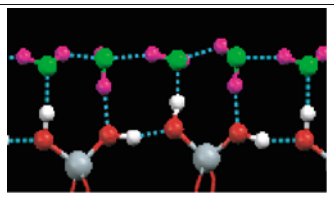
111	Pure Q^3	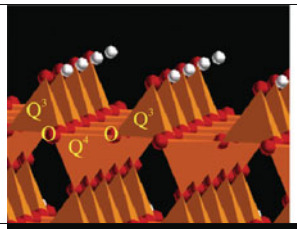	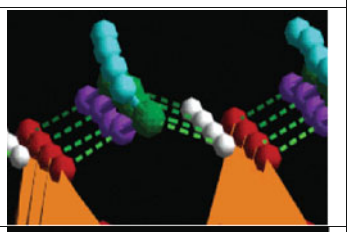
013	Q^2:Q^3 1:1 ratio	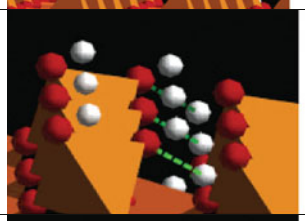	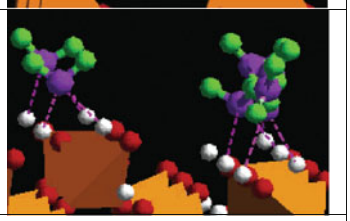
113	Q^2:Q^3 1:3 ratio	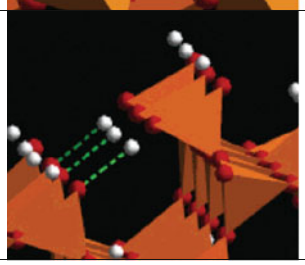	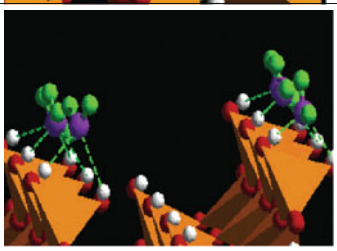

Fig. 4 Surface topology of {100}, {111}, {013}, and {113} β-cristobalite planes showing presence or lack of hydrogen bonding with and without the water overlayers

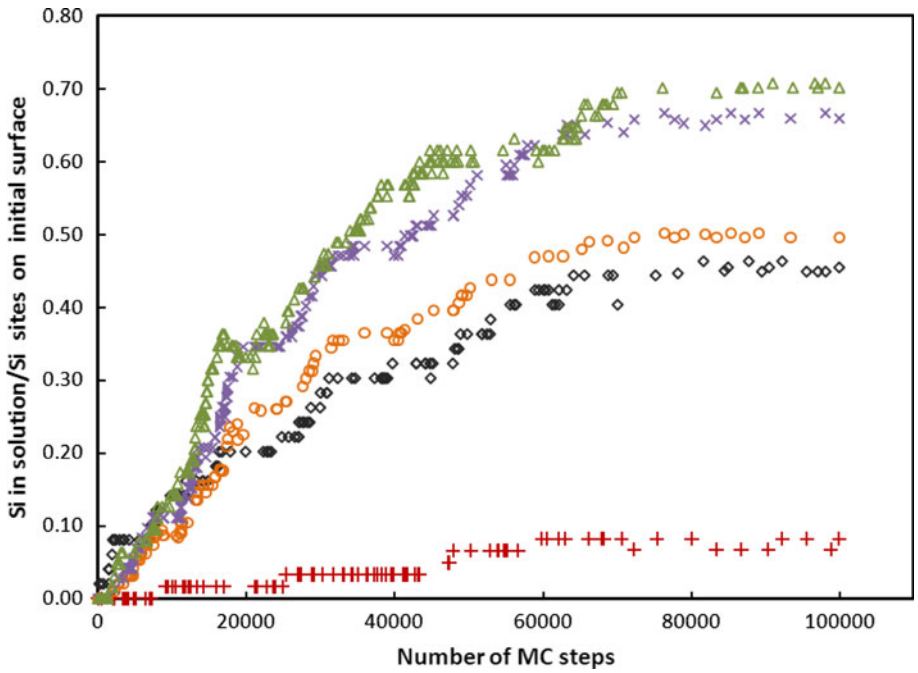

Fig. 5 Comparison of dissolution trends in plot of the ratio of the number of Si in solution to the number of Si sites in the initial surface versus number of MC moves for {100} (*plus*, *red*), {013} (*diamond*, *black*), {113} (*circle*, *orange*), {111} (*triangles*, *green*), and {110} (*cross*, *purple*). (The image is adapted from *J. Phys. Chem. C*, 2010, **114**, 2267–2272.)

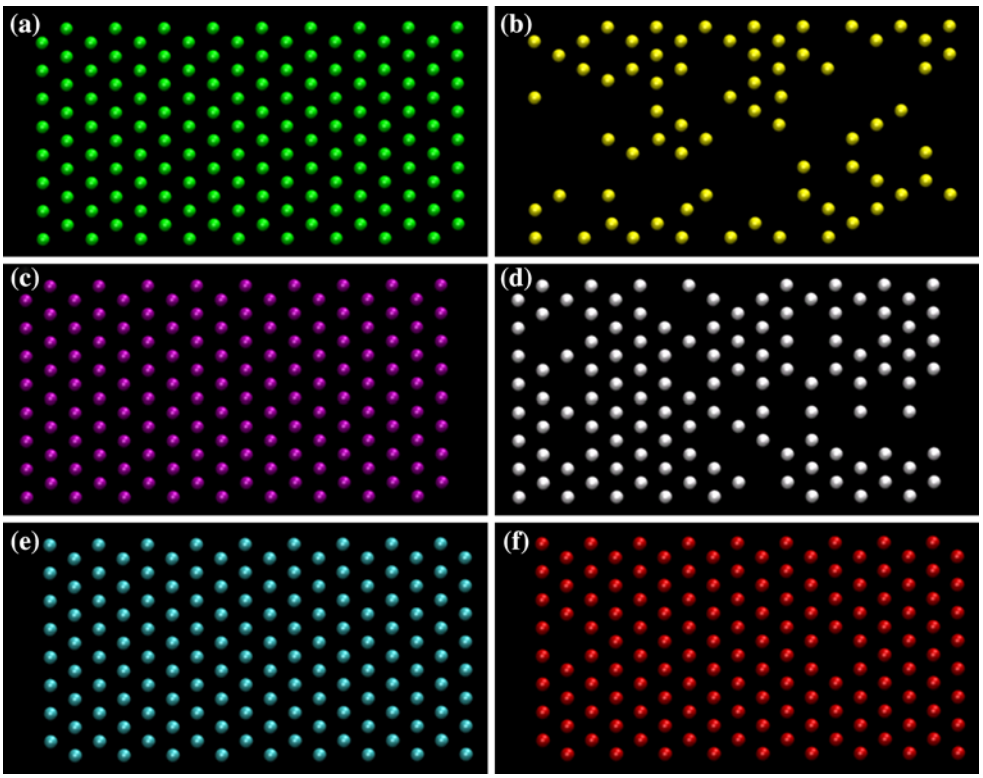

Fig. 6 Cross-sectional view of the {111} cristobalite surface showing only the Si atoms. *Panel* **a** top layer (*before*, *green*), **b** top layer (*after*, *yellow*) **c** second layer (*before*, *purple*), and **d** second layer (*after*, *white*), **e** third layer (*before*, *blue*), and **f** third layer (*after*, *red*). The atomic positions of O and H atoms are not shown for clarity. (The image is adapted from *J. Phys. Chem. C*, 2010, **114**, 2267–2272.)

described only the neutral reactions; therefore, the effect of pH on the dissolution process is not included. In the future, use of a more general silicate-water potential energy function can alleviate this restriction.

(d) The method cannot estimate the kinetics of the reaction, barrier height of the reactions, intermediate geometries, forward and backward rates.

The results of the RxMC-CBMC method for silicate dissolution are supplemented by studying the kinetics of the silicate-water system.

4 Kinetic studies

The kinetics of silicate–water dissolution provides information about the system that is complementary to the RxMC-CBMC methodology. The aim is to develop an affordable time-dependent method for evolution of the dissolution process far from equilibrium using accurate ab initio data and reaction rate constants. The reaction rate constants are incorporated in a kinetic Monte Carlo algorithm to describe dissolution of a three-dimensional silicate-water system.

Another important effect included in the silicate dissolution studies is the effect of pH. Based on the pH of the solution, silicate hydroxyl groups change their protonation state. The neutral hydroxyl group gets protonated or deprotonated in presence of hydronium ions or hydroxyl ions in solution. Earlier studies have shown that at any given pH, a specific ratio of the protonated, neutral, and deprotonated Q^i sites exists on the silicate surfaces [88]. To develop the kinetic Monte Carlo algorithm, the underlying ab initio data was obtained for a series of silicate clusters that undergo Q^1-dissolution.

4.1 Ab initio calculations

The ab initio calculations for the dissolution of Q^1 sites bridged to Q^2, Q^3, and Q^4 neighbors were performed for the series of reactions that are classified into the protonated, neutral, and deprotonated reactions [47, 48], as:

Protonated state

$$\left((\mathrm{OH})_3\mathrm{SiO}\right)(\mathrm{OH})_2\mathrm{Si}-\left[O-Si(OH)_3H\right]^+ + \mathrm{H_2O} \rightarrow \left((\mathrm{OH})_3\mathrm{SiO}\right)(\mathrm{OH})_2\mathrm{Si}-\mathrm{OH}+Si-(OH)_4H^+ \quad \text{(R1)}$$

$$\left((\mathrm{OH})_3\mathrm{SiO}\right)_2(\mathrm{OH})\mathrm{Si}-\left[O-Si(OH)_3H\right]^+ + \mathrm{H_2O} \rightarrow \left((\mathrm{OH})_3\mathrm{SiO}\right)_2(\mathrm{OH})\mathrm{Si}-\mathrm{OH}+Si-(OH)_4H^+ \quad \text{(R2)}$$

$$\left((\mathrm{OH})_3\mathrm{SiO}\right)_3\mathrm{Si} - \left[O - Si(OH)_3H\right]^+ + \mathrm{H_2O} \rightarrow \left((\mathrm{OH})_3\mathrm{SiO}\right)_3\mathrm{Si} - \mathrm{OH} + Si - (OH)_4H^+ \quad \text{(R3)}$$

Neutral state

$$\left((\mathrm{OH})_3\mathrm{SiO}\right)(\mathrm{OH})_2\mathrm{Si} - O - Si(OH)_3 + \mathrm{H_2O} \rightarrow \left((\mathrm{OH})_3\mathrm{SiO}\right)(\mathrm{OH})_2\mathrm{Si} - \mathrm{OH} + Si(OH)_4 \quad \text{(R4)}$$

$$\left((\mathrm{OH})_3\mathrm{SiO}\right)_2(\mathrm{OH})\mathrm{Si} - O - Si(OH)_3 + \mathrm{H_2O} \rightarrow \left((\mathrm{OH})_3\mathrm{SiO}\right)_2(\mathrm{OH})\mathrm{Si} - \mathrm{OH} + Si(OH)_4 \quad \text{(R5)}$$

$$\left((\mathrm{OH})_3\mathrm{SiO}\right)_3\mathrm{Si} - O - Si(OH)_3 + \mathrm{H_2O} \rightarrow \left((\mathrm{OH})_3\mathrm{SiO}\right)_3\mathrm{Si} - \mathrm{OH} + Si(OH)_4 \quad \text{(R6)}$$

Deprotonated state

$$\left((\mathrm{OH})_3\mathrm{SiO}\right)(\mathrm{OH})_2\mathrm{Si} - O - Si(OH)_2O^- + \mathrm{H_2O} \rightarrow \left((\mathrm{OH})_3\mathrm{SiO}\right)(\mathrm{OH})_2\mathrm{Si} - \mathrm{O}^- + Si(OH)_4 \quad \text{(R7)}$$

$$\left((\mathrm{OH})_3\mathrm{SiO}\right)_2(\mathrm{OH})\mathrm{Si} - O - Si(OH)_2O^- + \mathrm{H_2O} \rightarrow \left((\mathrm{OH})_3\mathrm{SiO}\right)_2(\mathrm{OH})\mathrm{Si} - \mathrm{O}^- + Si(OH)_4 \quad \text{(R8)}$$

$$\left((\mathrm{OH})_3\mathrm{SiO}\right)_3\mathrm{Si} - O - Si(OH)_2O^- + \mathrm{H_2O} \rightarrow \left((\mathrm{OH})_3\mathrm{SiO}\right)_3\mathrm{Si} - \mathrm{O}^- + Si(OH)_4 \quad \text{(R9)}$$

The three protonated states show distinct reactions profiles [47, 48]. The protonated and deprotonated reaction profiles both have two transition states indicating a two-step process, whereas the neutral reaction is a single transition state one-step reaction. A comparison of this data to prior data in the literature has been presented and discussed earlier [47, 48].

4.2 Calculations of rate constants

Using the barrier height of the reaction and the partition functions of the reactant and transition state at a given temperature, rate constants of a reaction using transition state theory (TST) were calculated. The TST expression for the rate constant is

$$k^{\neq}(T) = \frac{k_B T}{h}\frac{Q^{\neq}(T)}{Q(T)}e^{(-V^{\neq}/k_B T)} \quad (3)$$

where $V^{\neq}$ is the barrier height of the reaction, $Q^{\neq}$ is the partition function of the transition state, Q is the partition function of the reactants, k_B is Boltzmann's constants, h is Planck's constant, and T is the temperature. The TST expression in Eq. 3 was used to determine the k_p, k_n, and k_d rate constants for the protonated, neutral, and deprotonated reactions.

In our earlier work, we have used the rate constants information to calculate overall dissolution rates as a function of pH [47]. The equation for overall dissolution is

$$\text{rate} = \rho\left(k_\mathrm{p}\theta_\mathrm{p} + k_\mathrm{n}\theta_\mathrm{n} + k_\mathrm{d}\theta_\mathrm{d}\right) \quad (4)$$

Table 2 Comparison of quartz dissolution rates

pH	Log rate (mol m^{-2} s^{-1})		
	Ref. [88]	Ref. [47]	KMC
2	−13.0	−10.8	–
3	−13.0	−12.8	–
4	−12.3	−11.9	−12.6
5	−12.1	−11.7	−12.7
6	−10.9	−11.0	−11.9
7	−10.6	−10.9	−11.8
8	−10.5	−10.8	−11.9
9.4	−11.9	−11.4	–
10.1	−11.4	−11.1	–
11.0	−10.8	−10.8	–
12.2	−10.0	−10.6	–

where ρ is the molar surface density of reactive sites, θ_p, θ_n, and θ_d are the fractions of protonated, neutral, and deprotonated sites. For quartz, the total number of reactive surface sites (or surface hydroxyl groups) is 5–7 nm^{-2}. The rate of dissolution is expressed in the units of dissolution of the phase per surface area per unit time (mol m^{-2} s^{-1}). These surface fractions vary with pH and the calculated rates as a function of pH are listed in Table 2 [47].

4.3 Kinetic Monte Carlo

Another important aspect of the dissolution process is investigation of the overall rate of dissolution and identification of various intermediate species that have significant contribution of the dissolution process. Computer simulation of the time-dependent dynamical description can be performed by the chemical master equation method. In this approach, the master equation for the system is constructed from the rate equation of constituting reaction pathways. These equations result in a collection of coupled differential equations that are solved to obtain the time-propagation of the entire system. The solution of these equations gives the concentration of chemically active species as a function of time. For simpler systems, the chemical master equation can be solved analytically, but for complex processes (like dissolution) that involve large number of intermediates and reaction pathways, numerical methods are employed.

One of the vastly popular and successful techniques to solve the chemical master equation is the KMC method. Instead of solving the master equations using finite-difference schemes, this method employs a stochastic strategy. One of the earliest algorithms was formulated by Gillespie to solve the two component chemical master

equations [89]. The method outlined by Gillespie was readily extended for many-component system [90]. A general outline of the KMC scheme is presented below.

The KMC method assumes a priori knowledge of the reaction pathways and the corresponding rate constants. It also assumes that the initial concentrations of all the active chemical species are known. The first step of the KMC procedure involves calculation of all the reaction rates from the rate constants and initial concentrations. The cumulative reaction rate is obtained by summing over rates of individual reactions obtained in the previous step. In the third step, a reaction is selected using a random number such that the probability of selection is directly proportional to the rate of that reaction. The selected reaction is carried out by updating the concentrations of all the active species involved in the reaction according to their respective stoichiometry. The time step for this process is computed from the cumulative reaction rate and a random number between 0 and 1 using the following expression:

$$\Delta t = -\frac{\ln u}{R} \tag{5}$$

where R is the cumulative reaction rate, and u is a uniform random number between 0 and 1. The rates of all the reaction are then updated and the procedure is repeated. As the simulation progresses, the concentration of various chemical species and the chemical rates can be monitored as a function of time. Since its inception, there has been tremendous progress in the development of better and more efficient algorithms for carrying out KMC. For the present work, we implemented the scheme developed by Dooling and Broadbelt [90].

We applied our KMC method on a 10 Å quartz crystallite embedded in a cubic box of water of 50 Å dimension. The rate constants values for k_p, k_n, and k_d were 6.6×10^{-1}, 6.5×10^{-15}, and 8.9×10^{-5} that have been reported earlier [47]. The simulations were carried out in the pH range 4–8. A comparison of the rates reported earlier, and our KMC simulations are reported in Table 2, and a plot of the dissolution rates (mol m^{-2} s^{-1}) are plotted in the logarithmic scale as a function of pH in Fig. 7.

The preliminary data on a 10-Å quartz crystallite are promising, as the log of the dissolution rate with KMC is within one order of magnitude with the previously reported results. This result is crucial for the success of the KMC method for these kinds of systems that are dominated with different kinds of Q^i sites and varied surface topologies. In the present application, we have not used explicit rate constants for the dissolution of each of the Q^i sites in the protonated, neutral, and deprotonated state. The extension of this method to include more topological information in calculating the overall dissolution rates will be undertaken.

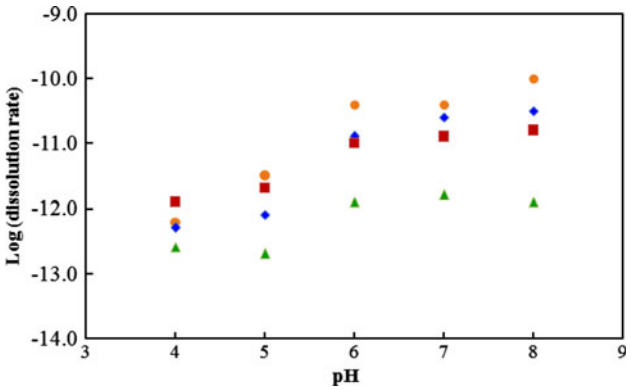

Fig. 7 Plot of the log(dissolution rate) of quartz as a function of pH at 298 K using four unique methods; experimental data by Knauss and Woolery (*circle*, *orange*, Ref. [88]), empirically fitted model by Dove and Elston (*diamonds*, *blue*, Ref. [88]), RxMC-CBMC method (*squares*, *red*, Ref. [47]), and KMC (*triangles*, *green*)

5 Discussion and conclusions

Geochemistry has primarily been an experimental science but with advances in computational tools and high performance computers there is promising theoretical development in this field. We developed two complementary approaches to simulate the dissolution of silicate–water systems at equilibrium and far from equilibrium. These methods are developed to provide a more comprehensive understanding the complexities of mineral–water interactions.

The dissolution and precipitation studies of silicate mineral have provided insight into the rich tapestry of the mineral structure. Some of the calculations have been performed using an interaction potential designed for neutral reactions, we believe that the topological argument should carry over to other conditions. For example, there are many polymorphs of silica with tetrahedral arrangements of SiO_4^{4-} units. Similarly, the protonation state changes depending on the pH, however, an extra or missing proton will not alter the basic topology. We propose that the same conclusions of role of hydrogen bonding on reactivity, tessellation of water overlayers, dominance of the Q^1-dissolution, and less frequent Q^2- and Q^3-stepwise dissolution events would apply for other polymorphs of silica as well as the protonated and deprotonated states. The generalized concepts that emerge from all the applications are given below.

Effect of surface topology on hydrogen-bonding tessellation; effect of tessellation on dissolution

(a) Most surfaces contain a mixture of Q^2 and Q^3 sites and on an average Q^3 centers are three times more abundant than the Q^2 centers. Crystallographic planes

with only Q^2 sites are rare whereas planes with only Q^3 centers are more frequent.

(b) The Q^2 sites have two hydroxyl groups that form intrasurface hydrogen bonds with adjacent surface sites. Crystallographic planes with higher percentages of Q^2 sites have a more extended hydrogen-bonding network than those with no Q^2 sites.

(c) The hydrogen bond network between surface groups tends to passivate the reactivity of crystallographic planes as demonstrated by the RxMC-CBMC simulations. Consequently, surfaces with higher percentages of Q^3 sites in the initial surface exhibit more dissolution than surfaces with higher percentages Q^2 sites.

(d) The interaction of surfaces with water overlayers depend on the topology of the surface. Surfaces with flat topology adsorb water molecules through hydrogen bonds that sometimes result in tessellated patterns. Tessellated patterns are not observed on corrugated surfaces.

Identification of dissolution and precipitation mechanisms

(e) The RxMC-CBMC method showed that dissolution and precipitation reactions occur via the stepwise mechanism predominantly from Q^1 sites resulting in a steady-state surface conformation. The dissolution of Q^1 sites occurs irrespective of the connectivity of the underlying Q^i site.

(f) The RxMC-CBMC approach ruled out the direct dissolution mechanism as realistic in which the Q^2 and Q^3 sites are proposed to undergo dissolution directly leading to silicic acid in solution.

(g) Stepwise dissolution of Q^2 and Q^3 sites are energetically expensive as they both lead to sterically crowded surface groups. These dissolution events occur less frequently than Q^1 dissolution.

pH affects: ab initio reaction profiles, rate constants, reaction rates, and overall dissolution

(h) The ab initio study of reaction mechanisms for the protonated and deprotonated species show similarity in the overall reaction profile with two transition states and a pentacoordinated intermediate. In contrast, the dissolution of the neutral species does not have a reaction intermediate but rather has a single transition state.

(i) The dissolution rates based on ab initio data over a wide 2–12 pH range compared well to three previously reported experimental rates. Also by using the same protonation site populations, our results are in good agreement with theoretically predicted rates that were obtained by fitting experimental data.

(j) The application of kinetic Monte Carlo technique using ab initio protonated, neutral, and deprotonated reaction rate constants provide an affordable method to study time evolution of silicate dissolution, especially because the dissolution process is slow and occurs over geological time scales.

The results presented here are for silicate minerals although the methodologies developed are general and can be extended to other mineral classes. The RxMC-CBMC method not only uses a suite of chemical reactions for simulation, so it can be applied to other minerals with a different set of reactions. Similarly, the kinetic Monte Carlo method can simulate other minerals using reaction rate constants for the key reactions for that mineral.

Acknowledgments We gratefully acknowledge the useful discussions with K. T. Mueller, J. D. Kubicki, and S. L. Brantley on this work. This project has been supported by the National Science Foundation NSF under the Grant Number CHE-0535656.

References

1. Chen Y, Brantley SL (1997) Chem Geol 135:275
2. Oelkers EH, Schott J, Devidal JL (1994) Geochim Cosmochim Acta 58:2011
3. House WAJ (1992) Chem Soc Faraday Trans 88:233
4. Bennett PC, Melcer ME, Siegel DI, Hassett JP (1988) Geochim Cosmochim Acta 52:1521
5. Bennett PC (1991) Geochim Cosmochim Acta 55:1781
6. Casey WH, Sposito G (1992) Geochim Cosmochim Acta 56:3825
7. Agger JR, Hanif N, Anderson MW (2001) Angewandte Chemie-Int Ed 40:4065
8. Anbeek C (1992) Geochim Cosmochim Acta 56:1461
9. Arvidson RS, Beig MS, Luttge A (2004) Am Mineral 89:51
10. Brady PV, Walther JV (1990) Chem Geol 82:253
11. Brantley SL (2004) Treatise Geochem 5:73
12. Carroll SA, Maxwell RS, Bourcier W, Martin S, Hulsey S (2002) Geochim Cosmochim Acta 66:913
13. Casey WH, Hochella MF Jr, Westrich HR (1993) Geochim Cosmochim Acta 57:785
14. Casey WH, Lasaga AC, Gibbs GV (1990) Geochim Cosmochim Acta 54:3369
15. Chuang I-S, Maciel GEJ (1996) Am Chem Soc 118:401
16. Dove PM (1995) Rev Mineral 31:235
17. Dove PM (1999) Geochim Cosmochim Acta 63:3715
18. Dove PM, Crerar DA (1990) Geochim Cosmochim Acta 54:955
19. Dove PM, Elston SF (1992) Geochim Cosmochim Acta 56:4147
20. Dove PM, Han N, Wallace AF, De Yoreo JJ (2008) Proc Natl Acad Sci USA 105:9903
21. Dove PM, Han N, Yoreo JJD (2005) PNAS 102:15357
22. Dove PM, Platt FM (1996) Chem Geol 127:331
23. Du Q, Freysz E, Shen YR (1994) Phys Rev Lett 72:238
24. Du Q, Freysz E, Shen YR (1994) Science 264:826
25. Fenter P, Sturchio NC (2004) Prog Surf Sci 77:171
26. Fry RA, Tsomaia N, Pantano CG, Mueller KTJ (2003) Am Chem Soc 125:2378
27. Fubini B, Zanetti G, Altilia S, Tiozzo R, Lison D, Saffiotti U (1999) Chem Res Toxicol 12:737
28. Gratz AJ, Bird P (1993) Geochim Cosmochim Acta 57:965

29. Ji N, Ostroverkhov V, Chen CY, Shen YR (2007) J Am Chem Soc 129:10056
30. Kinney DR, Chaung I-S, Maciel GEJ (1993) Am Chem Soc 115:6786
31. Luttge A, Bolton EW, Lasaga AC (1999) Am J Sci 299:652
32. McGuire JA, Shen YR (2006) Science 313:1945
33. Oelkers EH, Schott J (2001) Geochim Cosmochim Acta 65:1219
34. Ostroverkhov V, Waychunas GA, Shen YR (2005) Phys Rev Lett 94:046102
35. Rimstidt JD (1997) Geochim Cosmochim Acta 61:2553
36. Rimstidt JD, Barnes HL (1980) Geochim Cosmochim Acta 44:1683
37. Schwartzentruber J, Furst W, Renon H (1987) Geochim Cosmochim Acta 51:1867
38. Martin G, Garofalini SHJ (1994) Phys Chem 98:1311
39. VigneMaeder F, Sautet P (1997) J Phys Chem B 101:8197
40. de Leeuw NH, Higgins FM, Parker SC (1999) J Phys Chem B 103:1270
41. Pelmenschikov A, Strandh H, Pettersson LGM, Leszczynski J (2000) J Phys Chem B 104:5779
42. Lasaga AC, Luttge A (2004) Am Mineral 89:527
43. Lu ZY, Sun ZY, Li ZS, An LJ (2005) J Phys Chem B 109:5678
44. Yang JJ, Meng S, Xu LF, Wang EG (2005) Phys Rev B 71:23
45. Bandstra JZ, Brantley SL (2008) Geochim Cosmochim Acta 72:2587
46. Bickmore BR, Wheeler JC, Bates B, Nagy KL, Eggett DL (2008) Geochim Cosmochim Acta 72:4521
47. Nangia S, Garrison BJ (2008) J Phys Chem A 112:2027
48. Nangia S, Garrison BJ (2009) Mol Phys
49. Nangia S, Garrison BJ (2009) J Am Chem Soc 131:9538
50. Nangia S, Washton NM, Mueller KT, Kubicki JD, Garrison BJJ (2007) Phys Chem C 111:5169
51. Xiao Y, Lasaga AC (1996) Geochim Cosmochim Acta 60:2283
52. Xiao Y, Lasaga AC (1994) Geochim Cosmochim Acta 58:5379
53. Kubicki JD, Xiao Y, Lasaga AC (1993) Geochim Cosmochim Acta 57:3847
54. Lasaga AC, Gibbs GV (1990) Am J Sci 290:263
55. Yang J, Wang EG (2006) Phys Rev B 73:035406
56. Zhang Y, Li ZH, Truhlar DG (2007) J Chem Theory Comput 3:593
57. Criscenti LJ, Kubicki JD, Brantley SL (2006) J Phys Chem A 110:198
58. Feuston BP, Garofalini SHJ (1990) Phys Chem 94:5351
59. Feuston BP, Garofalini SHJ (1988) Chem Phys 89:5818
60. Feuston BP, Garofalini SH (1990) J Appl Phys 68:4830
61. Feuston BP, Garofalini SH (1990) Chem Phys Lett 170:264
62. Blonski S, Garofalini SH (1993) Surf Sci 295:263
63. Garofalini SH, Martin GJ (1994) Phys Chem 98:1311
64. Martin G, Garofalini SHJ (1994) Non-Crystalline Solids 171:68
65. Litton DA, Garofalini SH (2001) J Appl Phys 89:6013
66. Rao NZ, Gelb LD (2004) J Phys Chem B 108:12418
67. Mahadevan TS, Garofalini SH (2008) J Phys Chem C 112:1507
68. Lockwood GK, Garofalini SH (2009) J Chem Phys 131:074703
69. Rustad JR, Hay BP (1995) Geochem Cosmochim Acta 59:1251
70. Du ZM, de Leeuw NH (2006) Dalton Trans 2623
71. MacKerell AD Jr, Brooks B, Brooks CL III, Nilsson L, Roux B, Won Y, Karplus M (1998) CHARMM: the energy function and its parameterization with an overview of the program, vol 1. Wiley, Chichester
72. Lopes PEM, Murashov V, Tazi M, Demchuk E, MacKerell AD (2006) J Phys Chem B 110:2782
73. Lasaga AC, Luttge A (2005) J Phys Chem B 109:1635
74. Vinson MD, Luttge A (2005) Am J Sci 305:119
75. Yanina SV, Russo KM, Meakin P (2006) Geochem Cosmochim Acta 70:1113
76. Zhang L, Luttge A (2008) J Phys Chem B 112:1736
77. Smith WR, Triska B (1994) J Chem Phys 100:3019
78. Johnson K, Panagiotopoulos AZ, Gubbins KE (1994) Mol Phys 81:717
79. Siepmann JI, Frenkel D (1992) Mol Phys 75:59
80. Siepmann JI, McDonald IR (1993) Phys Rev Lett 70:453
81. Jakobtorweihen S, Hansen N, Keil FJJ (2006) Chem Phys 125:224709
82. Rosenbluth MN, Rosenbluth AW (1955) J Chem Phys 23:356
83. Yang J, Meng S, Xu LF, Wang EG (2004) Phys Rev Lett 92:146102
84. Léonardelli S, Facchini L, Fretigny C, Tougne P, Legrand APJ (1992) Am Chem Soc 114:6412
85. Tuel A, Hommel H, Legrand A (1990) Langmuir 6:770
86. Sindrof DW, Maciel GEJ (1983) Am Chem Soc 105:1487
87. Schlegel ML, Nagy KL, Fenter P, Sturchio NC (2002) Geochem Cosmochim Acta 66:3037
88. Dove PM (1994) Am J Sci 294:665
89. Gillespie DT (1976) J Comput Phys 22:403
90. Dooling DJ, Broadbelt LJ (2001) Ind Eng Chem Res 40:522